

Theoretical Model Construction of Deformation-Force for Soft Grippers Part II: Displacement Control Based Intrinsic Force Sensing

Huixu Dong, Ziyi Zheng, Haotian Guo, Sihao Yang, Chen Qiu, Jiansheng Dai, I-Ming Chen, *Fellow, IEEE*

Abstract—Compliant grasping is an essential capability for most robots in practical applications. For compliant robotic end-effectors that commonly appear in industrial or logistic scenarios, such as Fin-Ray gripper, it still remains challenging to build a bidirectional mathematical model that mutually maps the shape deformation and contact force. Part I of this article has constructed the force-displacement relationship for design optimization through the co-rotational theory with very few assumptions. In Part II, we further devise a detailed displacement-force mathematical model, enabling the compliant gripper to precisely estimate contact force sensor-free. Specifically, the proposed approach based on the co-rotational theory can calculate contact forces from deformations. The presented displacement-control algorithm elaborately investigates contact forces and provides force feedback for a force control system of a gripper, where deformation appears as displacements in contact points. Afterward, simulation experiments are conducted to evaluate the performance of the proposed model through comparisons with the finite-element analysis (FEA). Simulation results reveal that the proposed model accurately estimates contact force, with an average error of around 5% throughout all single/multiple node cases, regardless of various design parameters (Part I of this article is released in Google Drive¹).

Index Terms—Compliant gripper, Bidirectional modeling, Force sensing, Robotic grasp, Grasp performance

I. INTRODUCTION

COMPLIANT grasping plays an important role in robots' practical applications [1]–[3]. Despite significant progress in the field of compliant grasping, accurately sensing the forces involved in such grasps still presents a challenge as evidenced by existing literature [4]–[8]. Particularly, inadequate grasping forces may negatively influence grasping stability, even resulting in task failure. Meanwhile, excessive forces may cause damage to objects, especially fragile or soft ones. Therefore, it is well worth achieving the interaction forces between grippers and objects. Without loss of generality, we choose the Fin-Ray gripper as an example (see Fig. 1) that can be easily generalized to other compliant grippers.

Huixu Dong, Ziyi Zheng, Haotian Guo, Sihao Yang are with Robot Perception and Grasp Laboratory(Grasp Lab), Zhejiang University, Hangzhou 310058, China (e-mail: huixudong@zju.edu.cn). I-Ming Chen is with Robotics Research Center, Nanyang Technological University, Singapore 639798. Chen Qiu is with Maider Medical Industry Equipment Co., Ltd, China 317607. Jiansheng Dai is with Shenzhen Key Laboratory of Biomimetic Robotics and Intelligent Systems, SUSTech Institute of Robotics, Southern University of Science and Technology, Shenzhen, 518055, China, and Centre for Robotics Research, Department of Engineering, King's College London Strand, London WC2R 2LS, UK.

¹Part I: https://drive.google.com/file/d/1vQrXWIV_BwJNZCn5R654VdHE1HjYgqdq/view?usp=share_link

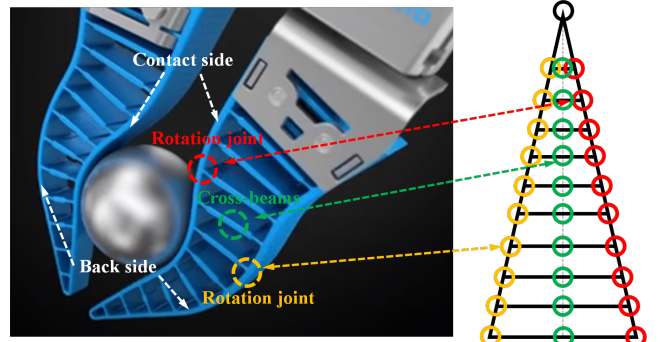


Figure 1: Festo's soft gripper based on Fin-Ray® effect and its equivalent fin-ray structure. The green circles represent the cross-beams; the yellow circles indicate the joints of the back side and the red circles are the joints of the contact side.

It poses a considerable challenge to obtaining the contact forces for a compliant grasp. Some force sensors based on force-sensitive resistors, strain gauges, and electrodes were developed and integrated into compliant grippers [9], [10]. However, in terms of stretchable deformations, it is not available for them to be attached to large-strain fingers, especially for soft grippers. A few new sensors appeared for obtaining contact forces of soft grippers based on the characteristics of capacitance or optical structures [11], [12], which also result in the complexity of compliant grippers. In addition, there exist good solutions for achieving contact forces through theoretical models of deformations and contact forces [13]–[16]. Such a model that reveals the deformation-force mathematical relationships is established by the pseudo-rigid body model [17], or Euler–Bernoulli bending method [18], [19] virtual work [15], [20], or piecewise constant curvature and Cosserat-rod theory [16], [21]–[23], or Newton–Euler iterations [24], or finite element method [25], [26], or two recent methods based on machine learning [14] and improved pseudo-rigid body model with the virtual work [13]. Xu et al. [14] introduced a neural network method to achieve the mapping relationships from the deformations to contact forces, skillfully avoiding building the corresponding model of compliant grasp; however, the learning-based approach has two limitations: effectiveness depends on the sample quality and quantity, and the model cannot be generalized to other scenarios. Additionally, changing the gripper geometry or size range makes the model ineffective. Also, they insert many rigid rods to modify the gripper structure, which improves gripper structure stiffness for the static model to be linear. Thus, this method is only suitable for linear-structured fin-ray

grippers. Shan et al. [13] proposed a theoretical model for deformation-force via an improved pseudo-rigid body model with the virtual work. However, this method's stiffness matrix assumes identical transformation frames or minor changes, the model cannot handle a scene where compliant fingers cause significant deformation. Shan's method can just tackle symmetrical-structure-compliant grippers, which is limited to broad applications. Moreover, these two methods are constrained to compliant grippers with fin-ray effects and rely on numerous assumptions for the deformation-force relationship.

To fill the above research gap, we seek to further construct the universal deformation-force model, providing crucial insights into design optimization and force control of fin-ray grippers. First, the proposed methods, based on the co-rotational theory, can map contact forces from deformations. The displacement control algorithm estimates contact forces and provides force feedback for a force control system of a gripper, where deformation appears as displacements in contact points. Second, a series of comparison simulations based on the proposed model and the standard FEA is implemented to evaluate the performance of the proposed model.

We highlight the novelties of this work. **Firstly**, this article, for the first time, explores the theoretical construction of the deformation-force relationship based on physical models through co-rotational concepts. **Secondly**, the individual influence of the co-rotational modeling parameters, namely mesh density and node radius factor, on the model's accuracy is first investigated. **Thirdly**, the comparison with FEA in simulation is innovatively adopted as FEA cannot provide contact force with the input displacement. This article will not only endow compliant grippers with a powerful mathematical tool that provides force perception, laying the groundwork for further research into theoretical model construction, but inspire more systematical and optimized gripper design.

The rest of the paper is organized as follows. We introduce the construction of the proposed model in section II. Section III describes the simulations for verifying the proposed theoretical model. The conclusion is drawn in Section IV.

II. MODELING AND ANALYSIS

A. Co-rotational Model

As demonstrated in Part I of this article, where any arbitrary large motion of objects can be accurately and efficiently modeled following the concept of the co-rotational modeling given by Crisfield [27] and Yaw [28], two algorithms are proposed, where **Algorithm 1** acquires the current pose of beam element, such as the current length \mathbf{L} , the cosine function \mathbf{c} of the incline angle β , the sine function \mathbf{s} of β , together with local internal force vector \mathbf{q}_l and internal global force vector \mathbf{F}_{int} , and **Algorithm 2** updates the modified global tangent stiffness matrix \mathbf{K}_s respectively. Besides, the force-deformation model, **Algorithm 3**, is devised for design optimization.

In particular, considering nodes or other hinge-type connections between the separate beam elements [29] in a real-world application, we introduce an index of effective length modification R_m and thus,

$$\begin{aligned} L_0 &= L_0 - 2R_m \\ L &= L - 2R_m \end{aligned} \quad (1)$$

The value of $R_m = \mu R_{node}$ is determined in terms of the connection shapes, with R_{node} the connection node radius and μ the modification factor, determined by comparison with the standard finite element simulation.

B. Displacement Control

“Displacement Control” indicates that the contact force is calculated by the displacement. In this section, a displacement control algorithm closely following controls schemes from McGuire et al. [30] and Clarke and Hancock [31] is provided, where a constantly increased external displacement load is applied at the target structure instead of an external force.

The details of the displacement control algorithm are as follows. Each node has three DoFs, including x-axis and y-axis translations and a rotation. If the maximum displacement for the x-axis or y-axis translation or the rotation is defined as a vector \mathbf{D}_{total} , and a total number n_{inc} of increments are required to reach the final equilibrium, we have

$$\Delta \bar{\mathbf{u}}_f = \frac{\mathbf{D}_{total}}{n_{inc}} \quad (2)$$

where $\Delta \bar{\mathbf{u}}_f$ represents an incremental value.

A full equilibrium cycle in the n -th increment is demonstrated. We obtain the modified stiffness matrix \mathbf{K}_s according to **Algorithm 1** and **Algorithm 2** based on the initial values resulting from the $(n-1)$ -th cycle. Then, a global nodal displacements vector can be calculated as

$$\hat{\mathbf{u}} = \mathbf{K}_s^{-1} \mathbf{F}_{ref} \quad (3)$$

where \mathbf{F}_{ref} is the referenced value [32]. The value of \mathbf{F}_{ref} is determined according to either experience or an automatic strategy. In our case, it is found that the direction of \mathbf{F}_{ref} is more important than its magnitude. As a result, the direction of \mathbf{F}_{ref} is set the same as \mathbf{D}_{total} . For the magnitude, we use a try-and-error approach. Then we can obtain the incremental load ratio vector $d\lambda^{n+1}$ as

$$d\lambda^{n+1} = \frac{\Delta \bar{\mathbf{u}}_f}{\hat{\mathbf{u}}} \quad (4)$$

And then update the load ratio [31]

$$\lambda^{n+1} = d\lambda^{n+1} + \lambda^n \quad (5)$$

Thus, the incremental force vector can be given as

$$d\mathbf{F} = d\lambda^{n+1} \mathbf{F}_{ref} \quad (6)$$

We calculate the incremental global nodal displacements as

$$d\mathbf{u} = \mathbf{K}_s^{-1} d\mathbf{F} \quad (7)$$

Then the global nodal displacements and global nodal forces can be updated as

$$\begin{aligned} \mathbf{u}^{n+1} &= \mathbf{u}^n + d\mathbf{u} \\ \mathbf{F}^{n+1} &= \mathbf{F}^n + d\mathbf{F} \end{aligned} \quad (8)$$

Further, we can update $\mathbf{L}, \mathbf{c}, \mathbf{s}, \mathbf{q}_l^{n+1}, \mathbf{F}_{int}^{n+1}$ according to **Algorithm 1** based on \mathbf{u}^{n+1} . By accounting for the required support, we calculate the residual as

$$\mathbf{R} = \lambda^{n+1} \mathbf{F}_{ref} - \mathbf{F}_{int}^{n+1} \quad (9)$$

The norm of the residual is provided as

$$R = \sqrt{\mathbf{R} \cdot \mathbf{R}} \quad (10)$$

Subsequently, we implement an iterative strategy to obtain the final values of the node displacement and externally applied force. A few iteration variables are defined as follows: Iteration number $k = 0$, tolerance $= 10^{-3}$. The maximum iteration

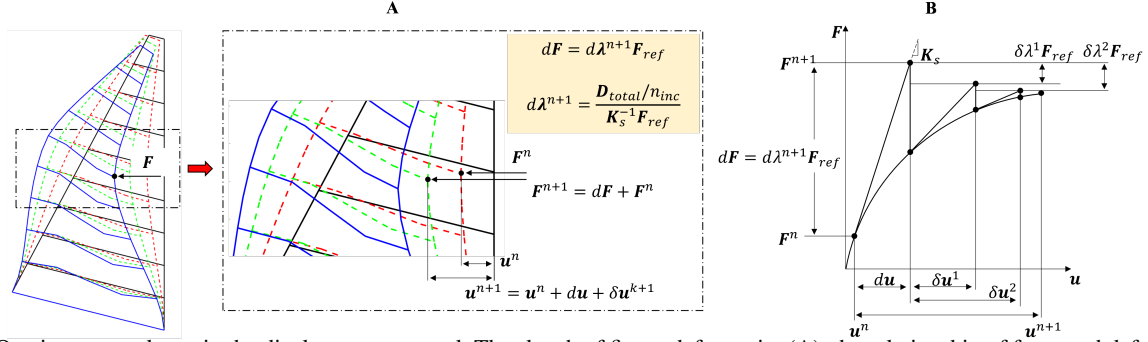


Figure 2: One incremental step in the displacement control. The sketch of finger deformation(A), the relationship of force and deformation(B).

step is limited by $maxiter = 100$. The correction to incremental global nodal displacements is defined as $\delta\mathbf{u}^k(\delta\mathbf{u}^0 = \mathbf{0})$, and the correction to load ratio is defined as $\delta\lambda^k(\delta\lambda^0 = \mathbf{0})$. The storage vector of local forces in this iteration cycle is set as $\mathbf{q}_{l-temp}^k = \mathbf{q}_l^{n+1}$.

In each step k , the stiffness matrix \mathbf{K}_s is updated according to **Algorithm 2** based on updated current values of inputs and \mathbf{q}_{l-temp}^k . The load ratio is calculated following [32] as

$$\begin{aligned}\dot{\mathbf{u}} &= \mathbf{K}_s^{-1}\mathbf{R} \\ \ddot{\mathbf{u}} &= \mathbf{K}_s^{-1}\mathbf{F}_{ref} \\ \delta\lambda^{k+1} &= \delta\lambda^k - \frac{\dot{\mathbf{u}}}{\ddot{\mathbf{u}}}\end{aligned}\quad (11)$$

Then the correction to \mathbf{u}^{n+1} can be calculated as

$$\delta\mathbf{u}^{k+1} = \delta\mathbf{u}^k + \mathbf{K}_s^{-1} \left[\mathbf{R} - \frac{\dot{\mathbf{u}}}{\ddot{\mathbf{u}}} \mathbf{F}_{ref} \right] \quad (12)$$

Update $\mathbf{q}_{l-temp}^{k+1}$ and \mathbf{F}_{int}^{n+1} according to **Algorithm 1**, and the residual in this iteration can be calculated as

$$\mathbf{R} = (\lambda^{n+1} + \delta\lambda^{k+1})\mathbf{F}_{ref} - \mathbf{F}_{int}^{n+1} \quad (13)$$

The norm of the residual is updated using Eqn.(10).

Then updating iteration number $k = k+1$, the iteration cycle will terminate if $R \leq tolerance$ or $k \geq maxiter$ (in this case, the convergence criteria are not met), and the variables will update to their final value in this n -th increment

$$\begin{aligned}\lambda^{n+1} &= \lambda^{n+1} + \delta\lambda^{k+1} \\ \mathbf{q}_l^{n+1} &= \mathbf{q}_{l-temp}^{k+1} \\ \mathbf{u}^{n+1} &= \mathbf{u}^n + \mathbf{du} + \delta\mathbf{u}^{k+1}\end{aligned}\quad (14)$$

The complete displacement control in the n -th increment is also illustrated in Fig. 2, where the variables updated in both the preliminary step and iteration cycle are demonstrated. The detailed algorithm is shown in **Algorithm 4**.

III. SIMULATION EXPERIMENTS

Simulation experiments were conducted to evaluate the performance of the proposed co-rotational approach by comparing it with the finite-element analysis (FEA), which is an important benchmark solution for the numerical analysis of mechanical models, providing displacements of elements subjected to an external force. Here a given compliant finger is meshed by rigid nodes, corresponding to the physical gripper in real scenarios, and detailed parameters are mentioned in Table I.

We apply a pre-defined external displacement load at the specified nodes (8 and 9) and generate contact forces estimation through the proposed co-rotational theory, which is later exerted on the same finger using FEA to generate nodal

Algorithm 4 Displacement Control

Input:

$n_{nodes}, n_{mem}, m_{conn}, \mathbf{A}, \mathbf{E}, \mathbf{I}, \mathbf{x}_0, \mathbf{y}_0, \mathbf{L}_0, \boldsymbol{\beta}_0, \mathbf{u}, R_m, D_{total}, \mathbf{F}_{ref}$

Calculations:

For $n=1: n_{mem}$

calculate $\Delta\ddot{\mathbf{u}}_f$ by Eqn.(2)

calculate $\dot{\mathbf{u}}$ by Eqn.(3)

calculate $d\lambda^{n+1}, \lambda^{n+1}$ by Eqns.(4-5)

calculate dF by Eqn.(6)

calculate $\mathbf{L}, \mathbf{c}, \mathbf{s}, \mathbf{q}_l, \mathbf{F}_{int}$ by **Algorithm 1**

calculate \mathbf{K}_s by **Algorithm 2**

calculate $d\mathbf{u}$ by Eqn.(7)

update \mathbf{u}^{n+1} and \mathbf{F}_{int}^{n+1} by Eqn.(8)

update $\mathbf{L}, \mathbf{c}, \mathbf{s}, \mathbf{q}_l^{n+1}, \mathbf{F}_{int}^{n+1}$ by **Algorithm 1** based on \mathbf{u}^{n+1}

calculate the residual \mathbf{R} and R by Eqns.(9-10)

set up iteration variables k , tolerance, $maxiter$, $\delta\mathbf{u}$, $\delta\lambda$ and \mathbf{q}_{l-temp}^k

start iterations while $R \geq tolerance$ and $k \leq maxiter$

i. calculate \mathbf{K}_s by **Algorithm 2**

ii. update load ratio correction $\delta\lambda^{k+1}$ by Eqn.(11)

iii. update $\delta\mathbf{u}^{k+1}$ by Eqn. (12)

iv. update $\mathbf{q}_{l-temp}^{k+1}, \mathbf{F}_{int}^{n+1}$ by **Algorithm 1**

v. calculate the residual \mathbf{R} by Eqn.(13), and its norm R by Eqn.(10)

vi. update iteration number $k=k+1$

End of while loop iterations

Update variables $\lambda^{n+1}, \mathbf{q}_l^{n+1}$ and \mathbf{u}^{n+1} by Eqn. (14)

End

Output: $\lambda^{n+1}, \mathbf{q}_l^{n+1}, \mathbf{u}^{n+1}$

Table I. The parameters of the sparsely and densely meshed models.

Items	Sparse	Dense
Node number	30	66
Member	38	74
Width m (m)	$40e^{-3}$	$40e^{-3}$
Height n (m)	$80e^{-3}$	$80e^{-3}$
Node radius R_{node} (m)	$0.75e^{-3}$	$0.75e^{-3}$
Node radius modification factor	1	0.5
Cross section of each member (b, h) (m)	$20e^{-3}, 1e^{-3}$	$20e^{-3}, 1e^{-3}$
Young's modules(Pa)	$2e^7$	$2e^7$

displacements since FEA simulation cannot read contact force. Two displacements are compared and Fig. 3 reveals a good agreement.

The rest of the section is organized as follows.

- 1) The effects of two representative co-rotational modeling parameters, such as the mesh density parameter and node radius factor, on the model's accuracy are investigated.
- 2) We further evaluate the performance of the co-rotational approach in estimating contact forces via the proposed displacement control.

Table II. Results of the evaluations of single-node force estimation. The values with blue background represent the average values with different nodes at the same displacement; the values with orange background denote the average values with the same nodes at different displacements; the green-background value is the total average value; the row with grey background has the invalid data (N.A.), which is not considered when an average value is calculated. Note that all the values are considered absolute values when average values are calculated.

	Dis. ¹	2mm	4mm	6mm	8mm	10mm		Dis. ¹	2mm	4mm	6mm	8mm	10mm	
Single-node	Node	Error ratio(%)					A. ² (%)	Node	Error ratio(%)					A. ² (%)
	1 st	-4	-13	-13	-10	N.A. ³	10	6 th	-4	-4	-4	-5	-5	4.4
	2 nd	-2	-3	-4	-5	-6	4	7 th	-3	-3	-3	-4	-4	3.4
	3 rd	-4	-4	-4	-5	-5	4.4	8 th	0	0	0	0	0	0
	4 th	-4	-4	-5	-5	-6	4.8	9 th	8	8	9	11	N.A. ³	9
	5 th	-4	-4	-5	-5	-5	4.6	A. ² (%)	3.00	3.14	3.57	4.14	4.43	3.66

Dis.¹ denotes the displacement; A.² indicates the average value; N.A.³ represents the FE method is invalid.

A. Co-rotational Modelling Parameter Comparison

1) Comparison in terms of the mesh density:

We first examine the effect of the number of meshed nodes on the performance of the proposed co-rotational approach. In the sparse model, we discretize the front/rear beam of a finger into nine flexible elements using ten nodes and the crossbeam into two flexible elements with one node (seen in Fig. 4), generating a total of 30 nodes. By contrast, the dense model adds one additional node in the flexible element of the sparse model, resulting in altogether 68 nodes.

The accuracy of both sparse and dense models in estimating forces is examined. For each model, nine nodes that physically exist on the front beam of the soft finger are selected, and a displacement load ranging from 2mm to 10mm is applied. Fig. 5 compares and illustrates the error ratios of both models. Generally, two models own similar error ratios at intermediate nodes (3,4,5,6,7) at various displacement loads except for the 10mm case. Meanwhile, we observe that the proposed method provides poorer performance at bordering nodes (1,2 and 8,9) regardless of the load magnitudes. However, since the most commonly used nodes are 3,4,5,6,7 in practical grasping scenarios, the influence of these negative results at node 1,2,8,9 can be minimized. It is worth noting that the dense model shows more consistent error ratios compared to those of the sparse model regarding the varying displacement-load magnitudes at various nodes. As a result, the co-rotational dense-meshed model is employed in the following simulations for its better performance.

2) Comparison of the node radius factor:

The node radius affects the accuracy of the co-rotational model in estimating contact forces. Inheriting the parameters set in the above dense-meshed model, we set three factors, 0.7, 0.6, and 0.5, to adjust the node radius in the simulation. The node radius affects the effective length of each beam. In particular, larger radius indicates a smaller effective length, resulting in a larger structural stiffness. Since the displacements of FEA simulation and co-rotational approach are compared at each node, the mathematical model with a larger node radius will have a smaller displacement at each node, thus the error line is higher (error line is the combination of error ratios at nine nodes). For the displacements from 2 to 10mm with the 2mm interval, the proposed co-rotational model with a radius factor of 0.7 has better performance than others, as shown in Fig. 6.

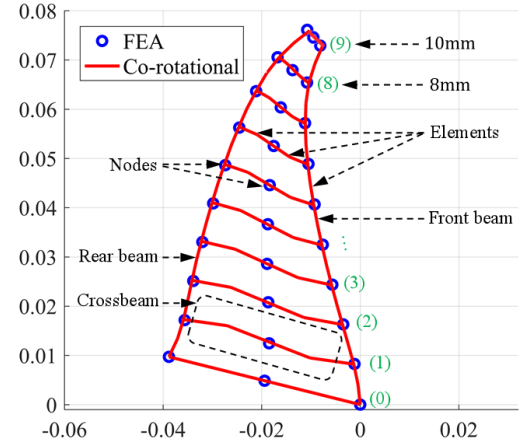


Figure 3: A comparison between the co-rotational modeling and FEA simulation. In this case, external displacement loads are applied at nodes 8 and 9. The deformation shape of the soft finger is described in the red line, and the FEA simulation result of key nodes is described in the blue circle, which shows a good agreement.

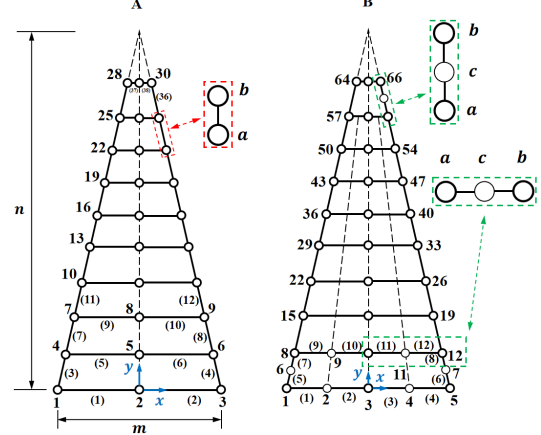


Figure 4: The models meshed sparsely (A) and densely (B). m and n represent the width and height of a fin-ray finger, respectively. The numbers indicate the labels of nodes, and the numbers in brackets denote the labels of flexible elements. The red frame with two nodes, a and b, represents the sparse connection style (A), where the bold circle indicates a physically existing node. For the dense connection style, an intermediate node c is introduced, which is a virtual node used in the analytical model.

B. Contact Force Estimation

The proposed approach is capable of estimating contact forces applied at the soft gripper by the developed displacement control algorithm, **Algorithm 4**. In addition, the parameters of the soft gripper are shown in Table I, except for

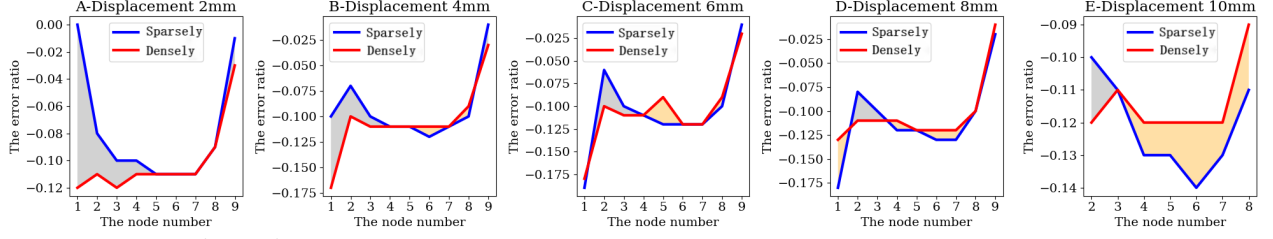


Figure 5: The models meshed sparsely (blue) and densely (red) in terms of mesh density.

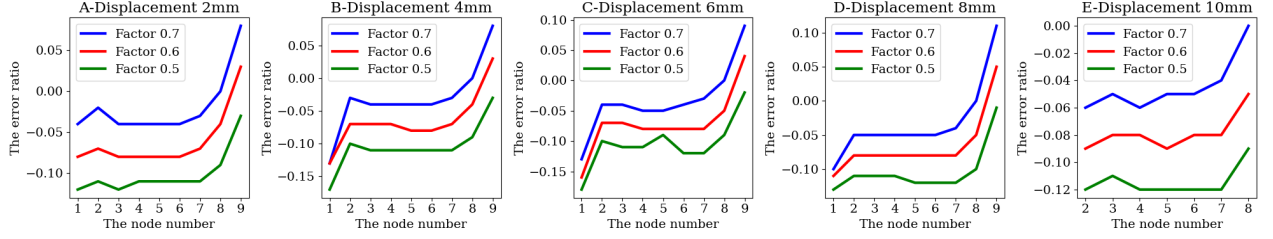


Figure 6: The error ratio of the densely meshed model with three node radius factors.

Table III. Results of the evaluations of two-node force estimation. The color notations are the same as Table II. The positive error ratios for node 9 are considered negative when the corresponding average values are calculated, as highlighted by the deep blue color.

	Dis. ¹ (mm)	(2,2)	(4, 4)	(6, 6)	(8, 8)	(10, 10)	
Two-adjacent nodes	Nodes			Error ratio(%)			Ave. ² (%)
	2+3	-1	-6	-4	-3	-4	4.80
	4+5	-8	-6	-6	-4	-6	5.70
	6+7	-3	-4	-3	-5	-5	4.30
8+9	-3	3	-1	6	-1	5	3.25
	Ave. ² (%)	3.75	4.75	3.50	4.50	3.50	4.75
Two-non-adjacent nodes	Nodes			Error ratio(%)			Ave. ² (%)
	2+8	-6	-1	-5	-2	-6	4.20
	4+7	-5	-4	-6	-4	-5	4.9
	Ave. ² (%)	5.50	2.50	5.50	3.00	5.50	4.50

Dis.¹ denotes the displacement; A.² indicates the average value; N.A.³ represents the FE method is invalid.

the node radius modification factor of 0.7 based on the above analysis.

1) Evaluation of the single-node cases:

Here we compare the proposed method's ability to estimate single-node force through experiments. Each node is subjected to a horizontal external displacement load, as indicated in Fig. 7. A 10mm-displacement can be considered a large deformation with respect to the dimension of the gripper. For nodes 1 and 9, since the FEA simulation is invalid for estimating forces with the 10mm displacements, the maximum applied displacement is set to be 8mm (see Table II). The reaction force obtained from the proposed method is applied to an FEA simulation with 14278 elements and large deflection, and the resulting displacement is compared with the original displacement load from the mathematical model. For a quantitative comparison, Table II indicates the rates of displacement discrepancies/errors from compared results predicted by the proposed model and the FEA method, respectively. The overall average estimation error rate is 3.66%. For the dense mesh model, displacement discrepancies are small (around 3%-4%) for displacements between 2mm to 10mm with 2mm intervals, indicating that the proposed method can accurately analyze the displacement-to-force (estimate the contact forces from displacements) of a fin-ray finger. Surprisingly, the displacement discrepancy does not appear to be roughly proportional to the displacement at a node, suggesting the mathematical model can predict the large deformation without sacrificing accuracy.

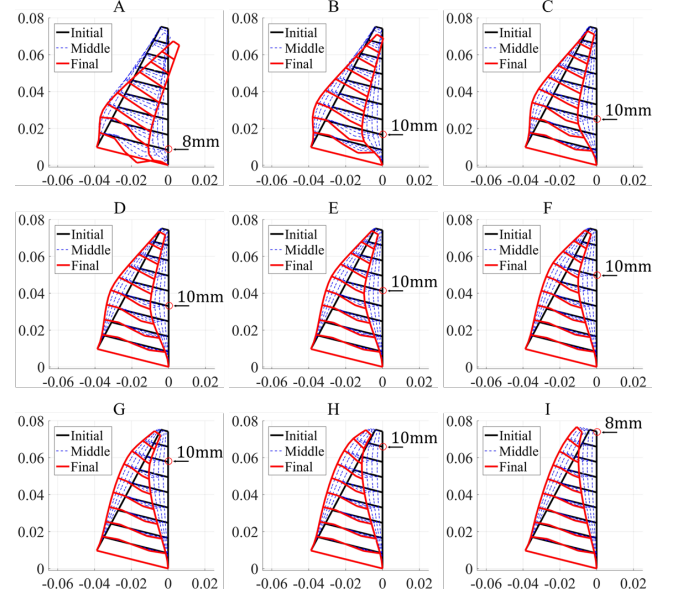


Figure 7: The deformations of a gripper for single-node displacement loads. Displacements at nodes 1(A), 2(B), 3(C), 4(D), 5(E), 6(F), 7(G), 8(H), 9(I).

The FEA simulation is invalid for estimating forces at the 10mm displacements at node 1 and node 9 (see Table II). Contrastively, the proposed model can deal with such cases. Actually, error ratios at these nodes are not considered when calculating average values, as they are not usually used for

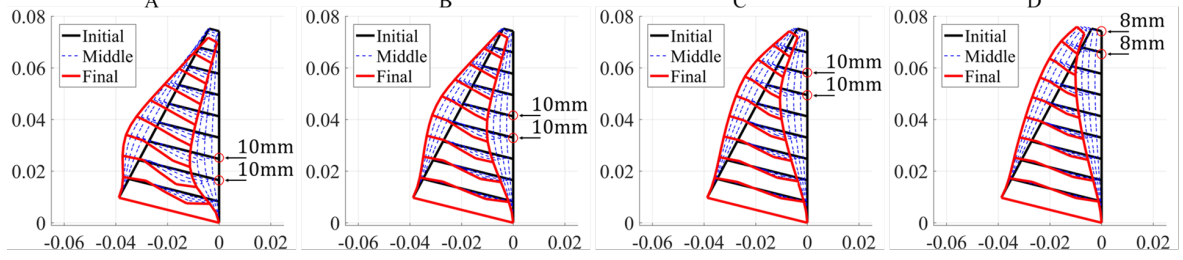


Figure 8: The deformations of a gripper for two-adjacent-node displacement loads.

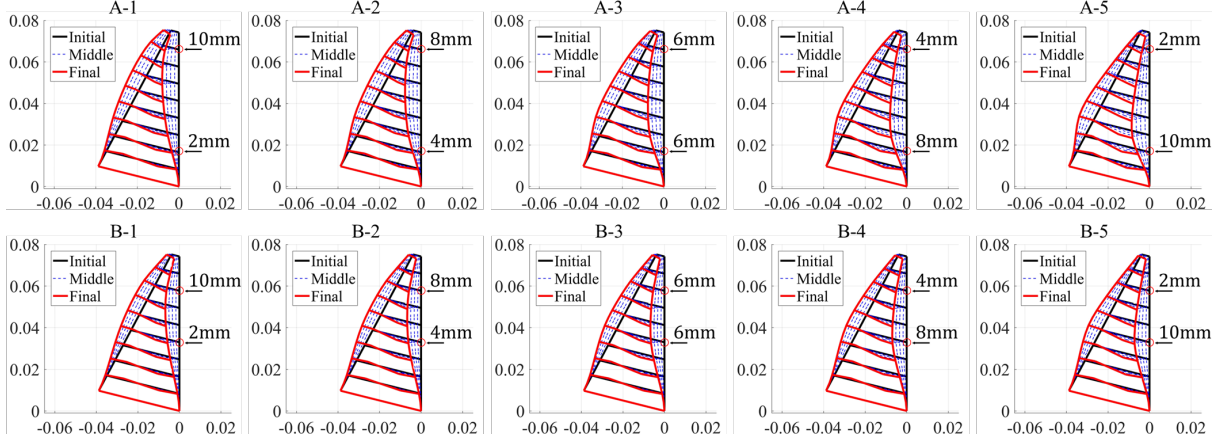


Figure 9: The deformations of a gripper for two-non-adjacent-node displacement loads at nodes 3, 9 (A), and 5, 8 (B).

contacting objects in gripper with fin-ray structure. They differ slightly for most displacement-force cases. In particular, these error ratios are very close, within 6% (Absolute value). Note that the proposed model demonstrates excellent consistency in terms of different positions and displacements. In particular, from node 3 to node 7, there are small fluctuations in displacement discrepancies at the same displacement. Moreover, displacements are gradually increased from 2mm to 10mm for all the nodes at the front beam; however, almost no obvious effect is generated on changing the displacement discrepancies/errors at the same node. At node 8, the proposed model illustrates an excellent performance with almost zero errors.

2) Evaluation of more than one-node cases:

(1) Displacements at two nodes

To evaluate the performance of the proposed method in estimating contact forces at two nodes, we conduct experiments focusing on the two-adjacent-node and two-non-adjacent-node cases. The setup of the simulations is similar to the above subsection, except that those two horizontal displacements are applied simultaneously at two selected nodes, as shown in Fig. 8 and Fig. 9. Statistical indicators of the force estimations from both the proposed model and the FEA method are illustrated in Table III. Therefore, it is reasonable to conclude that the proposed model can utilize finger deformations to accurately predict the contact forces when applied at two nodes. It is found that the proposed model can handle non-convergence at node 9 with 10mm displacement, while the FEA method fails, indicating the advantage of the proposed model over the FEA method.

Regardless of two-adjacent-node and two-non-adjacent-

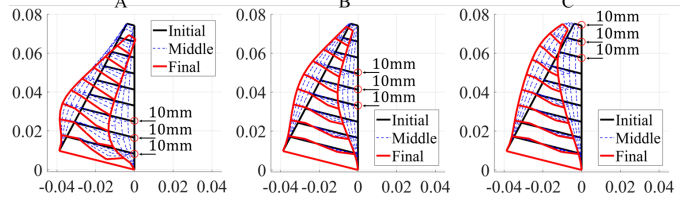


Figure 10: The deformations of a gripper for three-adjacent-node displacement loads.

node cases, the proposed method demonstrates a similar performance to the single-node case on the estimation accuracy, mostly maintaining around 4%-6% (absolute value) estimation errors for different positions and displacements. The reason is that the proposed model considers stiffness rather than a specific position. In terms of the two-adjacent-node cases, the corresponding average error ratios from the first group to the third group (i.e., from base to tip) are around 5% (see Fig. 8 and Table III). Moreover, in terms of two-non-adjacent-node cases, the discrepancy/error ratios at nodes (2 and 8) and (4 and 7) are less than 6% (see Fig. 9 and Table III). To sum up, the proposed approach is capable of sensing contact forces exerted on its middle part but has a poor performance when the contact points are near the tip or base, especially the tip. Moreover, the nonlinearity of the compliant finger results in a systemic error. For instance, the calibrated Young's modulus has a difference from the real one, which is a potential reason why the proposed model has a poor performance in estimating contact forces at the finger base and tip.

(2) Displacements at three nodes

We test the proposed approach in estimating forces at multiple nodes, focusing on three-node cases, including adjacent

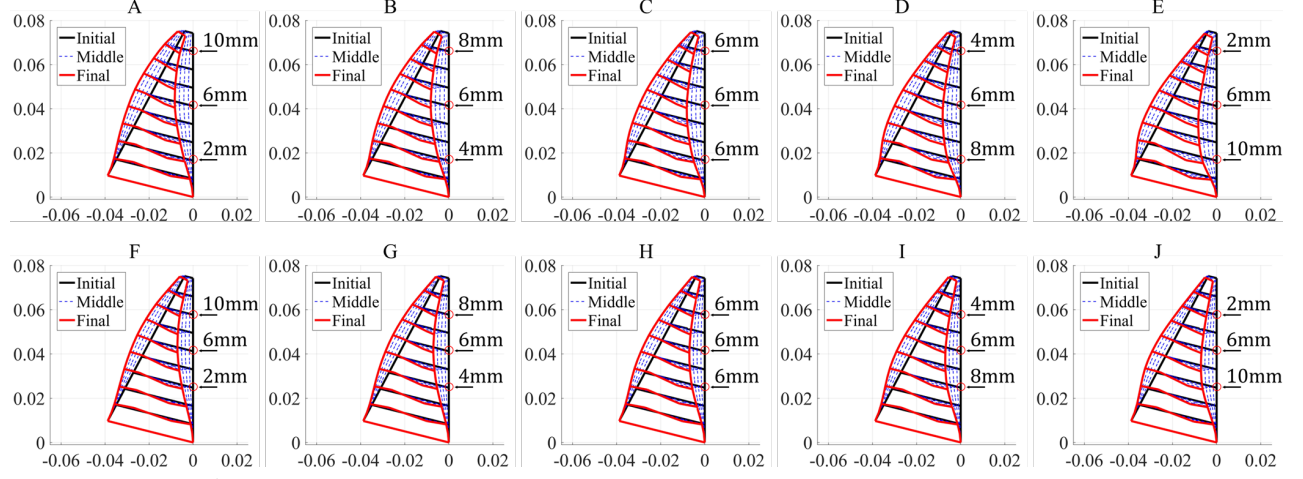


Figure 11: The deformations of a gripper for three-non-adjacent-node displacement loads.

Table IV. Results of the evaluations of three-node force estimation. The color notations are the same as Table III.

	Dis. ¹ (mm)	(2,2,2)	(4,4,4)	(6,6,6)	(8,8,8)	(10,10,10)	
3AN ³	Nodes				Error ratio(%)		
	1+2+3	-8	-3	-5	-6	-6	-9
	4+5+6	-7	-6	-4	-6	-4	-4
	7+8+9	-3	0	4	-3	0	-3
A-Ave. ² (%)	6	3	4	5	3	5	4
	6	3	4	5	3	5	4
3NAN ⁴	Dis. ¹ (mm)	(2,6,10)	(4,6,8)	(6,6,6)	(8,6,4)	(10,6,2)	
	Nodes				Error ratio(%)		
	2+5+8	-6	-6	-2	-6	-6	-5
	3+5+7	-5	-5	-4	-6	-5	-5
A-Ave. ² (%)	6	6	3	6	6	5	5
	6	6	3	6	6	5	5

Dis.¹ denotes the displacement; A-Ave.² indicates around average values; 3AN³ represents three-adjacent nodes; 3NAN⁴ represents three-non-adjacent nodes.

and non-adjacent nodes. The simulation comparison is similar, where three pre-defined horizontal displacement loads are applied at selected nodes simultaneously, and their reaction forces are recorded, as illustrated in Fig. 10 and Fig. 11. The comparison result suggests the average sensing error ratios are around 5%, which illustrates that the proposed model can well estimate forces at multiple nodes (see Table IV). Moreover, for force estimation on different positions and displacements, the proposed model shows excellent consistency, which is similar to the single-node cases.

The proposed model presents an unstable phenomenon in the first three-adjacent-node case, with the displacements gradually increasing. The high sensing error ratios at node 1 of the 8mm and 10mm displacements exceed 10% (absolute value). While for the middle parts (node 3 to node 9), the average error ratios are within 5%. One possible reason is that the joint points of the crossbeam and the beam have almost unchanged deformations at the finger base. In practical applications, inaccurate estimations at the base of the finger, where contact with the object is infrequent, will not significantly affect the actual grasp prediction. The estimating capability becomes better for estimating forces at three-non-adjacent-node cases without exceeding 5%, as shown in Table IV. The study demonstrates that the proposed model maintains good accuracy in estimating the contact forces with respect to large objects.

3) Discussions on the evaluation results:

It is supposed that the sources of these differences in this model are from a few aspects. First, the discretization degree based on the number of nodes meshing the model

causes the estimation error of the stiffness. Second, the shapes of the crossbeams tend to be “S”-shaped when undergoing large deformations of the finger, which brings in inaccurate estimations for stiffness matrixes in the model. Third, the deformation at the base (node 1) of the beam structure of compliant lengths generates a significant deformation compared with other locations, but it is difficult to obtain a precision measurement.

IV. CONCLUSIONS

In Part II of this article, detailed derivations of the displacement-force model have been devised to illustrate the intrinsic force-sensing principles behind the nonlinear deformation of grippers. We further explore the influence of modeling parameters on the algorithm’s performance in accuracy, and results indicate that a denser mesh and a bigger node radius factor are preferred. Meanwhile, the comparison with FEA simulations validates that the proposed displacement-force model can accurately and efficiently estimate the loaded forces, with an average error < 5%, regardless of various design parameters.

To sum up, this paper innovatively devises, demonstrates, and experimentally verifies a universal theoretical model that mutually depicts the bidirectional relationship between the gripper’s displacement and contact forces, facilitating both the optimization of gripper design and compliant grasping in a force-aware manner, sensor-free. Especially from the perspective of theoretical modeling, this work lays a solid foundation and provides a theoretical background for the development of more compliant grippers, providing a promising mathematical

tool for the control of soft fin-ray grippers and represents a first step toward a more effective design of more compliant grippers.

Future work will focus on the grasping experiments of the fin-ray gripper, where a gripper with two fin-ray-like fingers will be constructed, equipped with a camera that can capture shape deformations, to physically evaluate the performance and further validate the accuracy of the proposed model.

REFERENCES

- [1] H. Dong, E. Asadi, G. Sun, D. K. Prasad, and I.-M. Chen, "Real-time robotic manipulation of cylindrical objects in dynamic scenarios through elliptic shape primitives," *IEEE Transactions on Robotics*, vol. 35, no. 1, pp. 95–113, 2019.
- [2] H. Dong, D. K. Prasad, and I.-M. Chen, "Object pose estimation via pruned hough forest with combined split schemes for robotic grasp," *IEEE Transactions on Automation Science and Engineering*, vol. 18, no. 4, pp. 1814–1821, 2021.
- [3] H. Dong, E. Asadi, C. Qiu, J. Dai, and I.-M. Chen, "Geometric design optimization of an under-actuated tendon-driven robotic gripper," en, *Robotics and Computer-Integrated Manufacturing*, vol. 50, pp. 80–89, Apr. 2018.
- [4] J. Shintake, V. Cacucciolo, D. Floreano, and H. Shea, "Soft robotic grippers," *Advanced materials*, vol. 30, no. 29, p. 1707035, 2018.
- [5] F. Cini, V. Ortenzi, P. Corke, and M. Controzzi, "On the choice of grasp type and location when handing over an object," *Science Robotics*, vol. 4, no. 27, eaau9757, 2019.
- [6] V. Lippiello, B. Siciliano, and L. Villani, "A grasping force optimization algorithm for multiarm robots with multifingered hands," *IEEE Transactions on Robotics*, vol. 29, no. 1, pp. 55–67, 2012.
- [7] H. Dong, C.-Y. Chen, C. Qiu, C.-H. Yeow, and H. Yu, "Gsg: A granary-shaped soft gripper with mechanical sensing via snap-through structure," *IEEE Robotics and Automation Letters*, vol. 7, no. 4, pp. 9421–9428, 2022.
- [8] H. Dong, Y. Feng, C. Qiu, and I.-M. Chen, "Construction of interaction parallel manipulator: Towards rehabilitation massage," *IEEE/ASME Transactions on Mechatronics*, 2022.
- [9] J. Hashizume, T. M. Huh, S. A. Suresh, and M. R. Cutkosky, "Capacitive sensing for a gripper with gecko-inspired adhesive film," *IEEE Robotics and Automation Letters*, vol. 4, no. 2, pp. 677–683, 2019.
- [10] S. Aoyagi, M. Suzuki, T. Morita, T. Takahashi, and H. Takise, "Bellows suction cup equipped with force sensing ability by direct coating thin-film resistor for vacuum type robotic hand," *IEEE/ASME Transactions on Mechatronics*, vol. 25, no. 5, pp. 2501–2512, 2020.
- [11] H. Zhao, K. O'brien, S. Li, and R. F. Shepherd, "Optoelectronically innervated soft prosthetic hand via stretchable optical waveguides," *Science robotics*, vol. 1, no. 1, eaai7529, 2016.
- [12] C. Larson, B. Peele, S. Li, S. Robinson, M. Totaro, L. Beccai, B. Mazzolai, and R. Shepherd, "Highly stretchable electroluminescent skin for optical signaling and tactile sensing," *science*, vol. 351, no. 6277, pp. 1071–1074, 2016.
- [13] X. Shan and L. Birglen, "Modeling and analysis of soft robotic fingers using the fin ray effect," en, *The International Journal of Robotics Research*, vol. 39, no. 14, pp. 1686–1705, Dec. 2020.
- [14] W. Xu, H. Zhang, H. Yuan, and B. Liang, "A compliant adaptive gripper and its intrinsic force sensing method," *IEEE Transactions on Robotics*, vol. 37, no. 5, pp. 1584–1603, 2021.
- [15] K. Xu and N. Simaan, "An investigation of the intrinsic force sensing capabilities of continuum robots," *IEEE Transactions on Robotics*, vol. 24, no. 3, pp. 576–587, 2008.
- [16] V. A. Aloi and D. C. Rucker, "Estimating loads along elastic rods," in *2019 International Conference on Robotics and Automation (ICRA)*, IEEE, 2019, pp. 2867–2873.
- [17] V. K. Venkiteswaran and H.-J. Su, "A three-spring pseudorigid-body model for soft joints with significant elongation effects," *Journal of Mechanisms and Robotics*, vol. 8, no. 6, p. 061001, 2016.
- [18] L. U. Odhner and A. M. Dollar, "The smooth curvature model: An efficient representation of euler–bernoulli flexures as robot joints," *IEEE Transactions on Robotics*, vol. 28, no. 4, pp. 761–772, 2012.
- [19] F. Lotti, P. Tiezzi, G. Vassura, L. Biagiotti, G. Palli, and C. Melchiorri, "Development of ub hand 3: Early results," in *Proceedings of the 2005 IEEE International Conference on Robotics and Automation*, 2005, pp. 4488–4493.
- [20] A. Bajo and N. Simaan, "Hybrid motion/force control of multi-backbone continuum robots," *The International journal of robotics research*, vol. 35, no. 4, pp. 422–434, 2016.
- [21] R. J. Webster III and B. A. Jones, "Design and kinematic modeling of constant curvature continuum robots: A review," *The International Journal of Robotics Research*, vol. 29, no. 13, pp. 1661–1683, 2010.
- [22] F. Renda, M. Cianchetti, M. Giorelli, A. Arienti, and C. Laschi, "A 3d steady-state model of a tendon-driven continuum soft manipulator inspired by the octopus arm," *Bioinspiration & biomimetics*, vol. 7, no. 2, p. 025006, 2012.
- [23] D. C. Rucker and R. J. Webster III, "Statics and dynamics of continuum robots with general tendon routing and external loading," *IEEE Transactions on Robotics*, vol. 27, no. 6, pp. 1033–1044, 2011.
- [24] H. Yuan, P. W. Y. Chiu, and Z. Li, "Shape-reconstruction-based force sensing method for continuum surgical robots with large deformation," *IEEE Robotics and Automation Letters*, vol. 2, no. 4, pp. 1972–1979, 2017.
- [25] E. Coevoet, A. Escande, and C. Duriez, "Soft robots locomotion and manipulation control using fem simulation and quadratic programming," in *2019 2nd IEEE International Conference on Soft Robotics (RoboSoft)*, 2019, pp. 739–745.
- [26] Z. Zhang, A. Petit, J. Dequidt, and C. Duriez, "Calibration and external force sensing for soft robots using an rgb-d camera," *IEEE Robotics and Automation Letters*, vol. 4, no. 3, pp. 2356–2363, 2019.
- [27] R. De Borst, M. A. Crisfield, J. J. Remmers, and C. V. Verhoosel, *Nonlinear finite element analysis of solids and structures*. John Wiley & Sons, 2012.
- [28] L. L. Yaw, *Co-rotational meshfree formulation for large deformation inelastic analysis of two-dimensional structural systems*. University of California, Davis, 2008.
- [29] L. C. Hale, "Principles and techniques for designing precision machines," Lawrence Livermore National Lab.(LLNL), Livermore, CA (United States), Tech. Rep., 1999.
- [30] W. McGuire, R. H. Gallagher, and H. Saunders, "Matrix structural analysis," 1982.
- [31] M. J. Clarke and G. J. Hancock, "A study of incremental-iterative strategies for non-linear analyses," *International Journal for Numerical Methods in Engineering*, vol. 29, no. 7, pp. 1365–1391, 1990.
- [32] M. Crisfield, "A faster modified newton-raphson iteration," *Computer methods in applied mechanics and engineering*, vol. 20, no. 3, pp. 267–278, 1979.